Published April 24, 2006

Kinesin 5–independent poleward flux of kinetochore microtubules in PtK1 cells

Lisa A. Cameron,[1] Ge Yang,[2] Daniela Cimini,[1] Julie C. Canman,[1] Olga Kisurina-Evgenieva,[3] Alexey Khodjakov,[3,4] Gaudenz Danuser,[2] and E.D. Salmon[1]

[1]Department of Biology, University of North Carolina at Chapel Hill, Chapel Hill, NC 27599
[2]Laboratory for Computational Cell Biology, Department of Cell Biology, The Scripps Research Institute, La Jolla, CA 92037
[3]Wadsworth Center, New York State Department of Health, Albany, NY 12201
[4]Department of Biomedical Sciences, State University of New York at Albany, Albany, NY 12222

Forces in the spindle that align and segregate chromosomes produce a steady poleward flux of kinetochore microtubules (MTs [kMTs]) in higher eukaryotes. In several nonmammalian systems, flux is driven by the tetrameric kinesin Eg5 (kinesin 5), which slides antiparallel MTs toward their minus ends. However, we find that the inhibition of kinesin 5 in mammalian cultured cells (PtK1) results in only minor reduction in the rate of kMT flux from ~0.7 to ~0.5 μm/min, the same rate measured in monopolar spindles that lack antiparallel MTs. These data reveal that the majority of poleward flux of kMTs in these cells is not driven by Eg5. Instead, we favor a polar "pulling-in" mechanism in which a depolymerase localized at kinetochore fiber minus ends makes a major contribution to poleward flux. One candidate, Kif2a (kinesin 13), was detected at minus ends of fluxing kinetochore fibers. Kif2a remains associated with the ends of K fibers upon disruption of the spindle by dynein/dynactin inhibition, and these K fibers flux.

Introduction

Both kinetochore microtubules (MTs [kMTs]) and nonkMTs in mitotic and meiotic bipolar spindles of higher eukaryotes exhibit poleward translocation or flux (Rogers et al., 2005). Most kMTs normally extend the full length of the kinetochore fiber from their plus end attachment sites at kinetochores to minus end anchorage sites at spindle poles (McDonald et al., 1992). In animal cells, the flux of kMTs is coupled to minus end depolymerization at spindle poles. This poleward flux of kMTs can account for 20–100% of chromosome to pole movement depending on cell type (Rogers et al., 2005). The remaining poleward movement is produced by kinetochore "Pacman" motility that is coupled to kMT depolymerization at the kinetochore.

The molecular mechanisms that generate kMT poleward flux are still poorly understood. Several studies have reported that Eg5 (kinesin 5) is responsible for the sliding component of flux for both nonkMTs and kMTs (Miyamoto et al., 2004; Shirasu-Hiza et al., 2004; Goshima et al., 2005). This plus end–directed kinesin cross-links antiparallel MTs and slides them toward their minus ends. Because the plus ends of nonkMTs overlap with each other and with kMTs in the central region of a bipolar spindle, Eg5 is an ideal candidate for the role of flux driver. Forces could be applied to kMTs by interaction with Eg5 or through lateral cross-links to adjacent fluxing nonkMTs to the same pole (Margolis and Wilson, 1981; Maddox et al., 2003; Mitchison et al., 2004; Goshima et al., 2005). On the basis of these studies, Goshima et al. (2005) proposed a mechanistic model in which sliding forces generated by Eg5 drive poleward MT flux and activate MT minus end depolymerization at poles. A salient feature of this model is that pole-associated MT depolymerases (e.g., kinesin 13) sense sliding forces to regulate the depolymerization rate and spindle length. In agreement with this model, the inhibition of KLP10A (kinesin 13 in *Drosophila melanogaster*) did not affect the sliding component of flux but blocked depolymerization at the poles, resulting in highly elongated metaphase spindles (Rogers et al., 2004). In *Xenopus laevis* egg extract spindles, perturbation of the normal localization of Kif2a (kinesin 13) by the disruption of dynein/dynactin blocks MT minus end disassembly at poles, but antiparallel MT sliding continues (Gaetz and Kapoor, 2004).

Here, we test whether Eg5 is the dominant mechanism of kMT poleward flux in mammalian PtK1 cells using specific inhibitors of Eg5. We assay flux in monopolar spindles that lack antiparallel MTs and test two polar complex proteins for their

J.C. Canman's present address is Institute of Molecular Biology, University of Oregon, Eugene, OR 97402.

Correspondence to Lisa Cameron: lcameron@email.unc.edu; or E.D. Salmon: tsalmon@email.unc.edu

Abbreviations used in this paper: FSM, fluorescent speckle microscopy; kMT, kinetochore MT; MT, microtubule; PA, photoactivatable; qFSM, quantitative FSM.

The online version of this article contains supplemental material.

Supplemental Material can be found at:
http://jcb.rupress.org/content/suppl/2006/04/24/jcb.200601075.DC1.html

The Journal of Cell Biology, Vol. 173, No. 2, April 24, 2006 173–179
http://www.jcb.org/cgi/doi/10.1083/jcb.200601075

Published April 24, 2006

possible role in poleward flux. An important aspect of our studies is the use of quantitative fluorescent speckle microscopy (FSM [qFSM]) and fluorescence photoactivation techniques combined with two-color spinning disk confocal imaging to obtain much more accurate measurements for kMT poleward flux than achieved in previous studies on the roles of kinesin 5 and 13 for all spindle MTs (Miaymoto et al., 2004; Shirasu-Hiza et al., 2004; Ganem et al., 2005; Goshima et al., 2005).

Results and discussion

Kinetochores in mammalian cultured cells exhibit directional instability (Rieder and Salmon, 1998), although the character of movement is usually somewhat different for individual bioriented chromosomes at the spindle equator. Those chromosomes that are positioned near the spindle axis oscillate regularly between phases of poleward and antipoleward movement. In contrast, chromosomes aligned at the periphery of the metaphase plate show little, if any, oscillation (Khodjakov and Rieder, 1996; Cimini et al., 2004). We found by kymograph analysis that flux rates of kMTs were not significantly different for kinetochore fibers attached to oscillating and stationary chromosomes (Fig. 1, A–C; Video 1, and supplemental material, available at http://www.jcb.org/cgi/content/full/jcb.200601075/DC1). Although we consistently detected new speckles entering the kinetochore fiber as kMTs polymerized during antipoleward movement and detected the disappearance of speckles near the kinetochore as kMTs depolymerized during poleward movement (Fig. 1 B, arrows), the rates of flux remained constant (Fig. 1). The mean tension for stationary kinetochores as measured by the distance between sister kinetochores (2.6 ± 0.2 μm; $n = 30$ time points for each of seven kinetochores) was typically higher than the mean tension for oscillating sisters (2.36 ± 0.52 μm; $n = 30$ time points for each of six kinetochores; centromere rest length was 1.3 ± 0.25 μm in cells lacking MTs). Thus, the higher tensions developed at kinetochores as they stretched their centromeres during poleward movement for oscillating kinetochores had no detectable effect on the rate of kMT poleward flux in PtK1 cells, unlike what has been proposed in meiotic *Xenopus* egg extract spindles and crane fly spermatocytes (Maddox et al., 2003; LaFountain et al., 2004).

To improve the accuracy and statistical significance of our kMT flux measurements, we used qFSM (Danuser and Waterman-Storer, 2003). qFSM involves computer-vision methods to automatically detect and track speckles along kinetochore fibers (Fig. 1, I–K; supplemental material; and Fig. S1, A–C; available at http://www.jcb.org/cgi/content/full/jcb.200601075/DC1; Yang, G., A. Matov, and G. Danuser. 2005. Proceedings of the Institute of Electrical and Electronics Engineers International Conference on Computer Vision and Pattern Recognition. 9–17). This method yielded a mean kMT poleward flux velocity in bipolar spindles of 0.65 ± 0.08 μm/min ($n = 1{,}428$ tracks; supplemental material). The variation of speckle velocities within a spindle was larger (SD = 0.26 μm/min; Fig. 1 K) than between different spindles (supplemental material). This indicates that MT flux involves significant heterogeneity that is possibly associated with spatially and temporally varying contributions of multiple force-generation mechanisms. However, the flux pattern did not exhibit a clear spatial organization (Fig. 1 J), precluding the identification of the various sources of flux from heterogeneity analysis alone.

Kinetochore fibers are composed of ~25 kMTs and 25 nonkMTs in PtK1 cells (McEwen et al., 1998). The half-life of kMTs has been estimated to be ~5 min at metaphase, whereas the half-life of nonkMTs is much shorter (~0.2 min) because of the high dynamic instability of nonkMT plus ends and their rapid growth (11 μm/min) and shortening (~20 μm/min) velocities (Zhai et al., 1995; Tirnauer et al., 2002). The width of a kinetochore fiber (<0.4 μm) is not much larger than the resolution limit of the light microscope (0.25 μm). As a result, fluorescent speckles seen at a specific site in images of kinetochore fibers contain fluorophores from adjacent nonkMTs that produce fluctuation in speckle intensity that could potentially confuse automated tracking (supplemental material). Hence, we sought to verify flux rates by an independent method.

Tracking the movement of fluorescent marks on kMTs produced by photoactivation is less sensitive to signal instability caused by nonkMT turnover. Fluorescence from nonkMTs rapidly disappears after photoactivation (supplemental material and Video 2, available at http://www.jcb.org/cgi/content/full/jcb.200601075/DC1), leaving fluorescent marks on the more stable kMTs in higher contrast (Mitchison, 1989). We applied fluorescence photomarking methods to PtK1 cells expressing photoactivatable (PA) GFP (PA-GFP) fused to α-tubulin. PA-GFP–tubulin within spindle fibers was photoactivated by a 0.1-s pulse from a 408-nm laser focused by a cylindrical lens into a pseudo-Gaussian line profile with a 1.4-μm width at half-maximum intensity. The persistent marks on kinetochore fibers in metaphase cells were seen to move poleward at a constant velocity with a mean of 0.62 ± 0.26 μm/min (Video 2), which is similar to our qFSM measurements and earlier studies (Mitchison, 1989; Zhai et al., 1995). As reported previously (Mitchison, 1989; Zhai et al., 1995; Waters et al., 1996), the width of the mark along the fibers appeared relatively constant until it reached the ends of the kinetochore fibers at the pole, where it shortened at the velocity of poleward flux (Video 2). We simulated mark movements along the 5–7-μm length of kinetochore fibers in metaphase spindles using the velocity distributions obtained by qFSM (Fig. 1 K). These simulations produced movements of photoactivated marks that closely approximated the experimental data and indicated that the heterogeneity of speckle velocities does not detectably widen the mark over its short travel to the pole (supplemental material and Video 3).

To determine whether kMT poleward flux in PtK1 cells depends on the activity of kinesin 5, we used several specific small-molecule inhibitors. Monastrol (Miyamoto et al., 2004), HR22C16-E1 (Hotha et al., 2003), and s-trityl-L-cysteine (DeBonis et al., 2004) were used at concentrations reported to substantially inhibit flux in *Xenopus* egg extract spindles (100–200 μM monastrol) or induce monopolar spindles in mammalian cultured cells (10 μM HR22C16-E1 and 2 μM s-trityl-L-cysteine). Both qFSM and photoactivation approaches revealed that the inhibition of Eg5 in bipolar metaphase spindles did not abrogate kMT

Published April 24, 2006

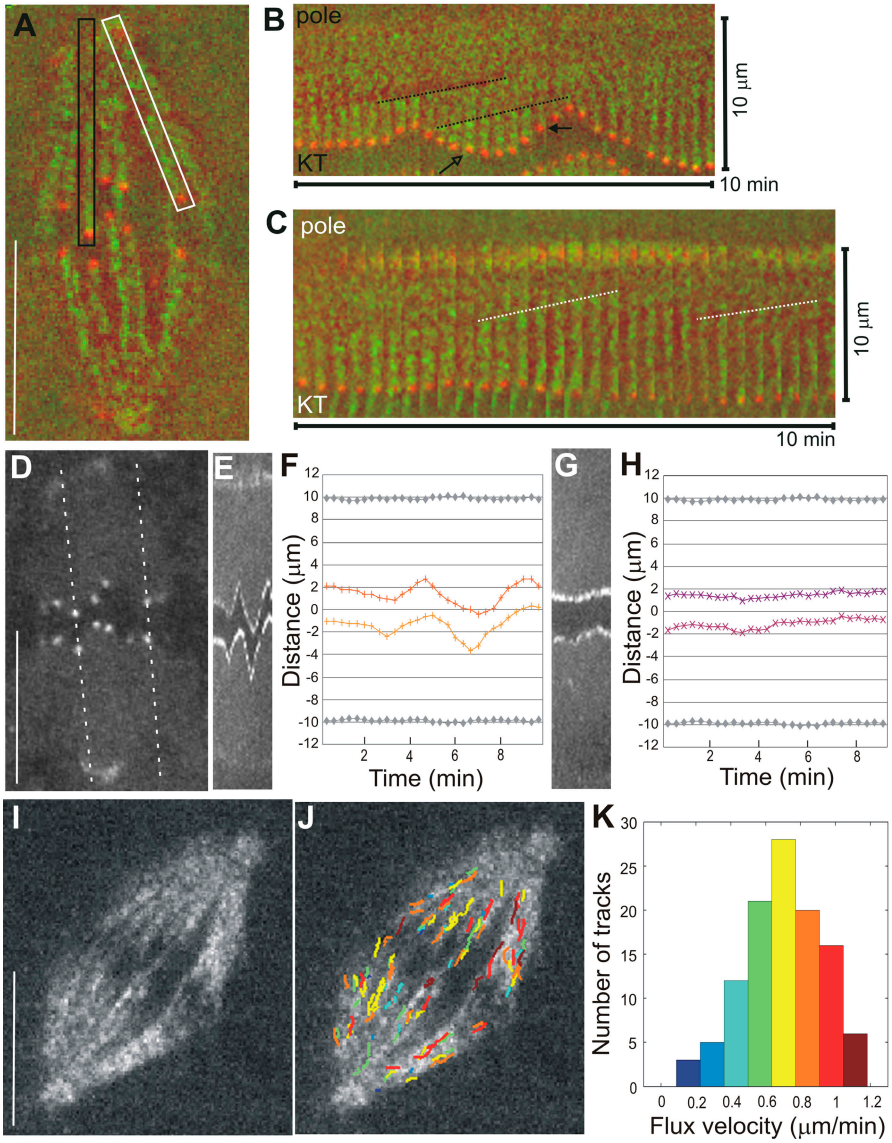

Figure 1. **Poleward flux and relative kinetochore movements in control PtK1 cells.** (A) Single frame from combined time-lapse sequence of tubulin (green) and CENP-F labeling of kinetochores and poles (red; Video 1, available at http://www.jcb.org/cgi/content/full/jcb.200601075/DC1). A fast Fourier transform filter set at high pass with a 20% cutoff in MetaMorph v4.5 was performed on the entire image sequence to help visualize fluorescent speckles above background. Black box denotes the region containing a MT kinetochore fiber, and its attached pole and kinetochore are shown in B. White box denotes the region shown in C. (B) Montage of cropped region from the interior of the spindle containing a kinetochore fiber and its attached pole and kinetochore. Each frame is 20 s apart; entire montage is 10 min from left to right. Maximum pole to kinetochore distance is 10 μm. Dotted lines follow the position of two speckles from frame to frame whose slopes indicate the rate of flux (0.6 and 0.7 μm/min, respectively). Open arrow denotes the time point at which the kinetochore is moving away from the pole and a new fluorescent speckle has incorporated into the kinetochore fiber. Closed arrow denotes the time point at which the kinetochore is moving poleward and "chewing up" a fluorescent speckle. (C) Montage of cropped region from the outer part of the spindle. Pole to kinetochore distance is 10 μm. The slopes of the dotted lines indicate a rate of speckle flux of 0.62 and 0.54 μm/min. (D) Single frame of fluorescently labeled CENP-F localized at the kinetochores and poles (same spindle as in A). Dotted lines show the location of the kymograph lines shown in E and G. (E) Kymograph of sister kinetochores in the interior of the spindle. (F and H) Kinetochore position (color) and pole position (gray) over time. (G) Kymograph of sister kinetochores at the spindle periphery. (I) Single frame of a time-lapse sequence showing a spindle imaged in FSM. (J) Frame in I overlaid with tracks of computer-detected speckle movement (color-coding according to the histogram in K). (K) Distribution of individual speckle velocities in J. Number of speckles tracked is 111; mean velocity is 0.70 ± 0.22 μm/min. Bars, 10 μm.

poleward flux, although the rate decreased by ~25% (to 0.5 ± 0.27 μm/min; Fig. 2 and see Fig. 5 A, supplemental material, and Videos 4 and 5; available at http://www.jcb.org/cgi/content/full/jcb.200601075/DC1). Spindle length and the character of chromosome movement also remained normal upon kinesin 5 inhibition (mean sister kinetochore distance = 2.16 ± 0.23 μm; either kinetochores with 20–30 time points each; P = 0.2, which is not significantly different from the control). Thus, Eg5 is responsible for only a minor contribution to kMT poleward flux during metaphase in PtK1 cells. This differs substantially from reports of kMT poleward flux and spindle length regulation in *Drosophila* S2 cells (Goshima et al., 2005) and MT flux in meiosis II *Xenopus* egg extract spindles (Miyamoto et al., 2004; Shirasu-Hiza et al., 2004) in which Eg5 has a dominant role.

Published April 24, 2006

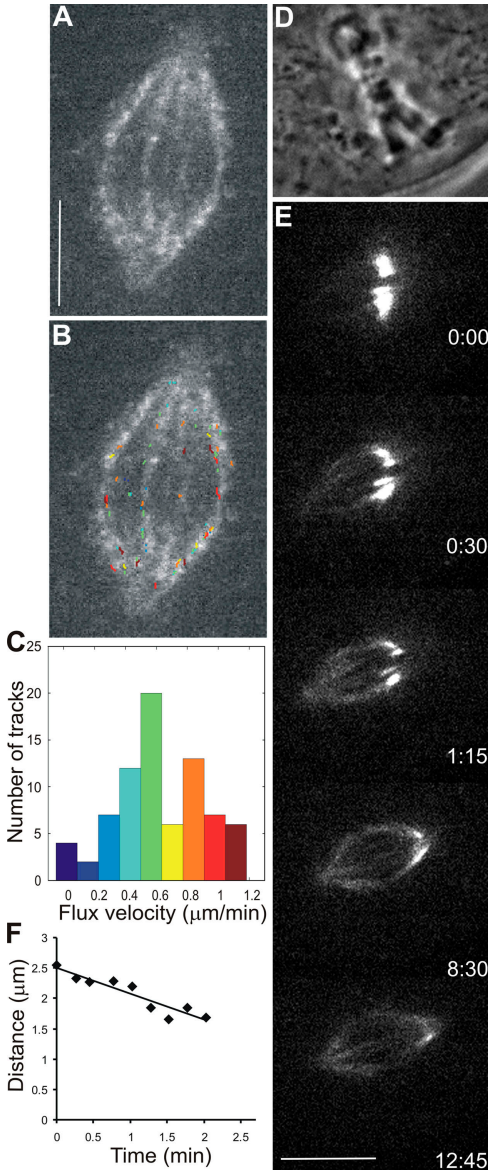

Figure 2. **Poleward flux in bipolar PtK1 cells treated with 200 μM monastrol.** (A) Single frame of FSM time-lapse sequence of the spindle in a PtK1 cell treated with monastrol (Video 4, available at http://www.jcb.org/cgi/content/full/jcb.200601075/DC1). Bar, 5 μm. (B) Image in A overlaid with computer-tracked speckle trajectories (color-coding according to histogram in C). (C) Distribution of individual speckle velocities in B. Number of speckles tracked is 77; mean velocity is 0.61 ± 0.30 μm/min. (D) Phase-contrast image of a PtK1 cell expressing PA-GFP–tubulin that was treated with monastrol. (E) Time series of fluorescence images showing photoactivated fluorescent mark of GFP-tubulin (Video 5). Time in minutes/seconds is given in the bottom right corner of each image. Bar, 10 μm. (F) Distance between the distal end of mark and pole versus time. Slope indicates kMT flux rate of 0.43 μm/min.

Although Eg5 is thought to be the molecule responsible for antiparallel MT sliding, it is conceivable that other molecular motors can contribute to this mechanism. Therefore, we analyzed kMT poleward flux in monopolar spindles that do not have overlapping MTs of opposite orientation. The addition of kinesin 5 inhibitors before nuclear envelope breakdown results in the formation of monopolar spindles with unseparated centrosomes (Kapoor et al., 2000). Plus ends of MTs in the monopolar spindles are uniformly oriented away from the pole, as evident from time-lapse recordings of PtK1 cells expressing the GFP form of the +TIP protein EB1 (Fig. 3 A and Video 7, available at http://www.jcb.org/cgi/content/full/jcb.200601075/DC1; Tirnauer et al., 2002). Chromosomes attach to monopolar spindles via either one (monotelic) or both sister kinetochores (syntelic) and oscillate toward and away from the pole in a normal fashion (Video 6; Tirnauer et al., 2002).

The rate of kMT poleward flux in monopole spindles measured by qFSM was 0.56 ± 0.1 μm/min (n = 7 cells; 792 tracks; Fig. 3, B–D). We also measured flux in monopoles using photoactivation of a bar of fluorescence across a monopolar spindle in between the chromosomes and the pole (Fig. 3 F). Much as in bipolar spindles, photoactivated marks disappeared quickly for nonkMT fibers and persisted for fibers containing kMTs. These persistent marks moved poleward at a constant velocity (Fig. 3 G) until they reached the ends of their kinetochore fibers. Then, the width of the mark decreased at the rate of flux (Fig. 3, Fig. S1 E, and Video 8, available at http://www.jcb.org/cgi/content/full/jcb.200601075/DC1). Photoactivation measurements yielded a velocity of poleward flux of 0.44 ± 0.26 μm/min (n = 13 cells; 17 tracks; see Fig. 5 A and supplemental material). Thus, when Eg5 is inhibited, the velocity of flux is similar between monopolar and bipolar spindles. This, in turn, implies that most of kMT poleward flux in mammalian spindles is not based on the sliding of antiparallel MTs.

Recently, Ganem et al. (2005) reported that MT poleward flux in bipolar mitotic spindles is inhibited by siRNA depletion of the depolymerase Kif2a in human U2OS cells. These cells were also depleted of another depolymerase, mitotic centromere-associated kinesin, which alone did not block flux. In this study, they were unable to resolve kinetochore fibers. In PtK1 cells, we found that Kif2a was concentrated at the polar minus ends of kinetochore fibers from late prometaphase through anaphase, and it also localized to centromeres throughout mitosis and to centrosomes during interphase and mitosis (Fig. S2, available at http://www.jcb.org/cgi/content/full/jcb.200601075/DC1). Microinjection of antibodies to either human or *Xenopus* Kif2a into prophase or prometaphase cells had no effect on the progression of chromosome alignment or segregation as assayed by live cell imaging (unpublished data). Because siRNA for Kif2a is currently not possible in PtK1, we attempted to alter Kif2a localization at spindle poles by microinjecting a recombinant protein fragment (p150_CC1) of the NH_2-terminal coil-coiled domain of the $p150^{Glued}$ subunit of dynactin. P150_CC1 disrupts dynein/dynactin, induces spindle lengthening, and has been shown to greatly diminish Kif2a localization to spindle poles in *Xenopus* egg extract spindles (Gaetz and Kapoor, 2004). In PtK1 cells, p150_CC1 microinjection altered spindle morphology, causing centrosomes to become disconnected from the ends of the spindle and minus ends of kinetochore fibers to become less focused (Fig. 4 and Fig. S2). Nevertheless, poleward flux continued in both bipolar (0.70 ± 0.08 μm/min; Video 9) and monopolar spindles, and Kif2a remained most concentrated at the minus ends of the kinetochore fibers (Fig. 4). In addition, most sister chromosomes continued to oscillate as assessed by themovement of dark bars (absence of fluorescence) between growing and shortening sister kinetochore fiber pairs (Video 9).

Published April 24, 2006

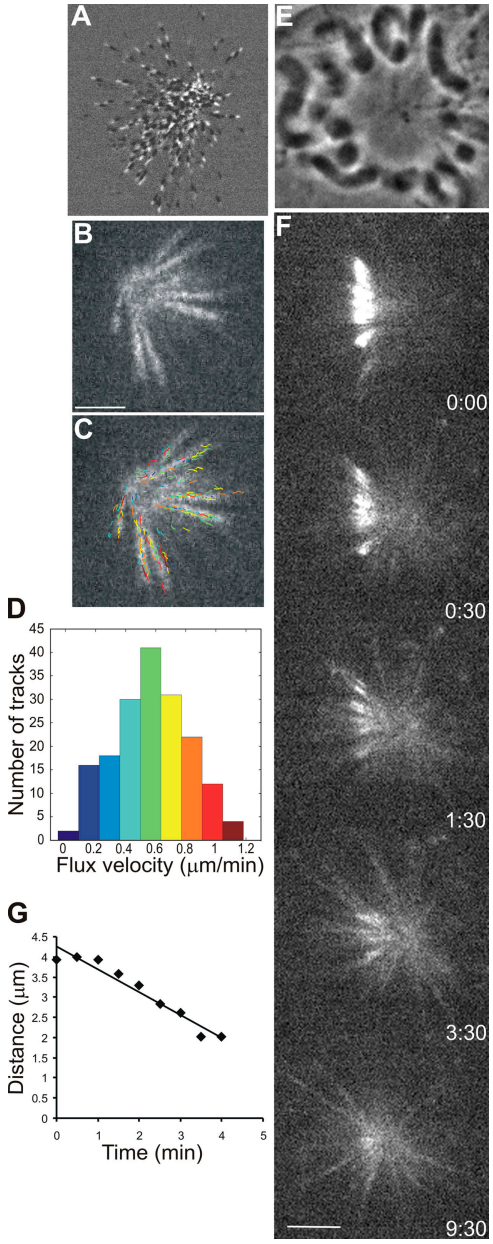

Figure 3. **Poleward flux in monopolar PtK1 cells treated with monastrol.** (A) PtK1 cell expressing GFP-EB1 treated with 200 μM monastrol (Video 7, available at http://www.jcb.org/cgi/content/full/jcb.200601075/DC1). Image 2 was subtracted from image 1 in MetaMorph software to show the direction of EB1 movement. White mark exterior to black mark shows that MT plus ends are oriented away from the pole. (B) FSM frame of a PtK1 cell treated with 100 μM monastrol (Video 6). (C) Frame in B overlaid with computer-tracked speckle trajectories (color-coding according to the histogram in D). (D) Distribution of individual speckle velocities in C. The number of speckles tracked is 176; mean velocity is 0.57 ± 0.24 μm/min. (E) Phase image of monopolar spindle in a PtK1 cell expressing PA-GFP–tubulin treated with 200 μM monastrol. (F) Time series of fluorescence images showing the photoactivated fluorescent mark of GFP-tubulin (Video 8). Time in minutes/seconds is given in the bottom right corner of each image. (G) Distance between the distal end of mark and pole versus time. Slope indicates a MT flux rate of 0.56 μm/min. Bars, 5 μm.

These results indicate that Kif2a is an integral part of a complex of proteins that concentrates at the minus ends of individual, fluxing kinetochore fibers even when the minus ends of the fibers are not attached to the centrosome and are not focused together.

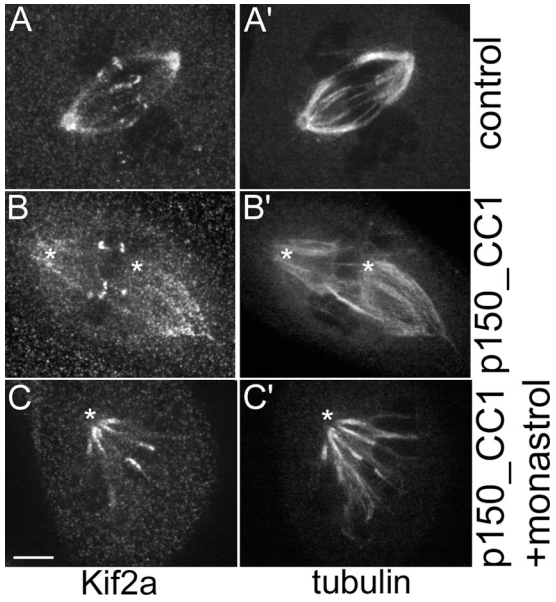

Figure 4. **Localization of Kif2a in control and p150_CC1-injected PtK1 cells.** Control bipolar spindle showing Kif2a (A) and tubulin (A′) localization. (B) Cells injected with p150_CC1 and rhodamine-tubulin were then fixed and stained for Kif2a. Tubulin (B′) is from the injected rhodamine-tubulin signal. (C) Cells treated with 200 μM monastrol and injected with p150_CC1 and tubulin showing the localization of Kif2a (C) and tubulin (C′) in the monopolar spindle. Images are the addition of two planes of a z series in which each pole is most in focus. Asterisks denote the position of the centrosome as found in other planes of the z series. Bar, 5 μm.

Our results reveal that neither Eg5 nor antiparallel MTs are required for the majority of kMT poleward flux in PtK1 cells. The velocity of flux in PtK1 cells is slow relative to flux in *Drosophila* embryo and *Xenopus* egg extract spindles, and there is little (Goshima et al., 2005) to no (Mitchison et al., 2004) flux in monopolar spindles in these systems. These results suggest that mechanisms responsible for flux contribute differently in different systems (e.g., mammals vs. lower animals).

Although polar ejection forces on chromosome arms push nonkMTs poleward, they pull kinetochores and their kMTs away from the pole (Rieder and Salmon, 1998). As a result, polar ejection forces cannot be the source of force that produce a constant rate of kMT poleward flux in monopolar spindles, particularly during kinetochore poleward movement when kinetochores pull strongly on their kMTs in a direction opposite to flux.

Instead, our data indicate that in PtK1 cells, the dominant mechanism of kMT poleward flux is a poleward pulling-in mechanism coupled to minus end depolymerization (Fig. 5 B; Margolis and Wilson, 1981; Sawin and Mitchison, 1991; Waters et al., 1996; Chen and Zhang, 2004; Ganem et al., 2005). This mechanism may be similar in principle to the kinetochore Pacman mechanism. However, the mechanism of dynamic attachment and pulling force generation at a depolymerizing end is not well understood. It might involve sleeve mechanisms as envisioned by Hill (1985), rings of DASH/DAM proteins like those discovered in budding yeast, anchorage proteins like NuMA, and pulling forces generated by inside-out peeling of tubulin protofilaments at depolymerizing ends promoted by the ATPase activity of depolymerases like Kif2a (Salmon, 2005).

Published April 24, 2006

Our p150_CC1 data suggest that a kind of self-feeding mechanism is working in which both the depolymerase and pulling activity are in the same complex that remains at minus ends of K fibers and does not require anchorage to the centrosome or focused pole. Flux and depolymerization rates may depend critically on load, as proposed by Goshima et al. (2005). A plus end–directed kinesin motor attached to the complex of proteins at the minus ends of kinetochore fibers may be critical for driving poleward flux (Sawin and Mitchison, 1991) as well as reducing the load on the depolymerization mechanism ("thresher mechanism"). Sensitivity of the minus end depolymerization mechanism to load would also explain how kinesin 5–driven sliding forces in bipolar PtK1 spindles produce a 25% increase in the poleward flux rate of kMTs.

Finally, we found little change in the length of bipolar spindles when Eg5 was inhibited, a result typical for mitotic mammalian spindles in late prometaphase or metaphase (Kapoor et al., 2000). Unlike meiosis II spindles in *Xenopus* egg extracts, other factors such as astral or polar ejection forces may play a much more significant role in determining metaphase spindle length than Eg5 sliding forces.

Materials and methods

Cell culture

PtK1 cells were maintained in Ham's F-12 medium (Sigma-Aldrich) and were complemented with 10% FBS, antibiotics, and antimycotic (Cimini et al., 2004). A PtK1 cell line stably expressing PA-GFP fused to α-tubulin was created by selecting cells transfected with a vector that was made by removing α-tubulin with BamHI and XhoI from the GFP-tubulin vector (CLONTECH Laboratories, Inc.) and ligating it into pPA-GFP-C1 (gift of G. Patterson and J. Lippincott-Schwartz, National Institute of Child Health and Human Development, Bethesda, MD; Patterson and Lippincott-Schwartz, 2002). PA-GFP–tubulin PtK1 cells were selected with 1 mg/ml geneticin and maintained in Ham's F-12 as PtK1 cells except they were sometimes complemented with 15% FBS to promote the growth and health of cells. A PtK1 cell line stably expressing GFP-EB1 was a gift of J. Tirnauer (University of Connecticut Health Center, Farmington, CT) and was maintained in Ham's F-12 with 0.25 mg/ml geneticin. For live cell imaging, all cells were incubated in Leibovitz's L-15 (Invitrogen) complemented with 10% FBS, antibiotics, antimycotic, 7 mM Hepes, 4.5 g/L glucose, and 0.45 U/ml oxyrase (Oxyrase).

Microinjection and microscopy

We used two-color fluorescence live cell imaging. PtK1 cells were coinjected with low levels of X-rhodamine–labeled tubulin to fluorescently speckle MTs (Waterman-Storer et al., 1998) and AlexaFluor488-labeled antibodies to CENP-F protein (gift of D. Cleveland [University of California, San Diego, San Diego, CA] and T. Tafari [National Institute of Environmental Health Sciences, Research Triangle Park, NC]) to label kinetochores and spindle poles (Cimini et al., 2004). Microinjection was performed at room temperature to prevent tubulin polymerization inside the microneedle. For dynein/dynactin inhibition experiments, 0.2 μg/ml p150_CC1 recombinant protein (needle concentration; gift of J. Gaetz and T. Kapoor, The Rockefeller University, New York, NY) was coinjected with rhodamine-labeled tubulin (to designate which cells were injected for the immunofluorescence of Kif2a or for speckle labeling of MTs in live cell imaging experiments to measure flux rates). Some cells were injected with tubulin alone and fixed and stained for Kif2a (human antibody to Kif2a was a gift of D. Compton, Dartmouth Medical School, Hanover, NH; *Xenopus* antibody to Kif2a was a gift of R. Ohi, Harvard Medical School, Boston, MA) to ensure that rhodamine-tubulin injection was not altering Kif2a localization. Tubulin and antibody or p150_CC1 were diluted into tubulin injection buffer (50 mM K-glutamate and 0.5 mM $MgCl_2$, pH 7.0, with KOH) and coinjected into prophase and/or early prometaphase cells. Digital images were collected with a cooled CCD camera (Orca ER; Hamamatsu) coupled to a Yokogawa spinning disk confocal unit (CSU10; PerkinElmer), which was attached to an inverted microscope (TE300; Nikon [Cimini et al., 2004]) with a 100× 1.4 NA plan-Apochromatic differential interference contrast objective. Stage temperature was maintained at ∼35°C using an air curtain incubator (ASI 400; Nevtek). Near simultaneous fluorescence images were acquired at 488 and 568 nm at a single focal plane every 5–20 s. For photoactivation, a 408-nm laser (56ICS323; Melles Griot) was focused by a cylindrical lens into a pseudo-Gaussian line profile with a 1.4-μm width at half-maximum intensity. Images were collected before and after a 0.1-s photoactivation through a 100× 1.4 NA plan-Apochromatic phase objective to track chromosome and spindle location (phase contrast) and the photoactivated bar (488-nm fluorescence and 1-s exposure).

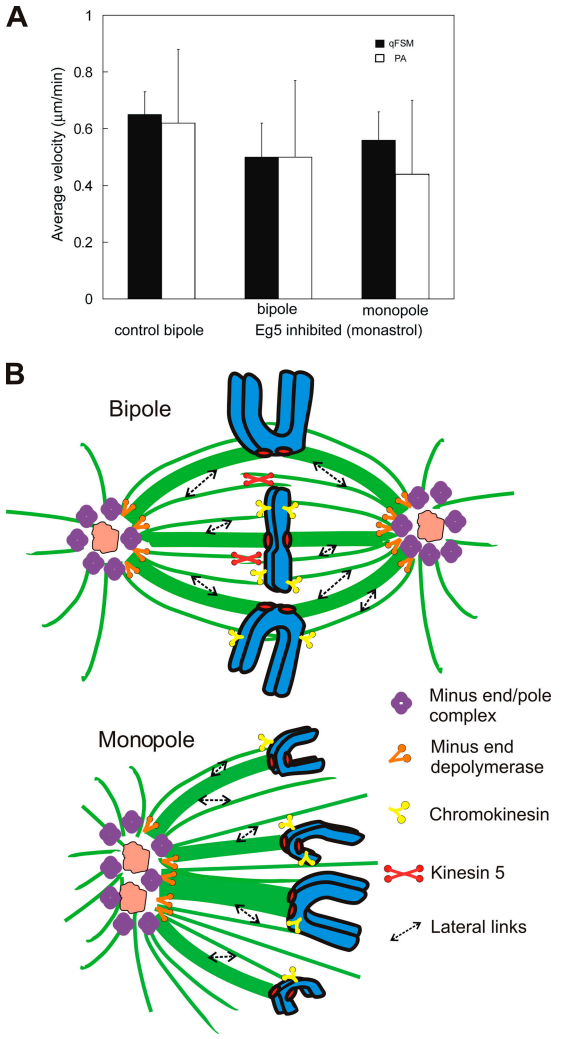

Figure 5. **Summary of flux measurements and model.** (A) Bar graph comparing the flux rate in control, kinesin 5–inhibited bipoles, and monopoles using qFSM (black bars) and photoactivation (white bars). Error bars are the SD between spindles. (B) Model of spindle components contributing to poleward flux in bipolar and monopolar PtK1 cells.

Speckle tracking and data analysis

Each frame of the FSM image sequence was aligned to the previous frame in the sequence using a correlation-maximization algorithm (Pratt, 2001). Speckle detection was then performed on the aligned images as previously described (Ponti et al., 2003). Speckle tracking was formulated as a modified optimal bipartite graph linear assignment problem and was solved using the Jonker-Volgenant algorithm (Yang, G., A. Matov, and G. Danuser. 2005. Proceedings of the Institute of Electrical and Electronics Engineers International Conference on Computer Vision and Pattern Recognition. 9–17). The flux rate for each track was defined as its mean velocity. When computing flux rates in a specific region, only those tracks that were contained completely within that region were considered.

Published April 24, 2006

Software for image alignment, speckle detection, speckle tracking, and statistical analysis of tracking results was developed using MATLAB (Mathworks) and C++. For photoactivation image analysis, the distance between the photoactivated mark and the closest pole was tracked and measured over the time course of the video using MetaMorph software (Molecular Devices). A graph of distance versus time was plotted, and the slope of the best-fit line was determined to be the flux rate for that mark.

Online supplemental material

Online supplemental material includes methods for fluorescent speckle detection and tracking, a simulation of photoactivation, and additional analysis of flux velocity distributions in monastrol-treated cells. Fig. S1 shows an example of speckle tracking (A–C) and a cumulative velocity histogram comparison (D). Fig. S1 E is a kymograph corresponding to the monopolar spindle in Fig. 3 F. Fig. S2 shows the localization of Kif2a and the effects of p150_CC1 injection in PtK1 cells. Table 1 contains a summary of all poleward flux measurements. Video 1 corresponds to Fig. 1 (A–C). Video 2 shows a photoactivated mark of tubulin fluorescence moving to the pole in a control spindle. Video 3 shows four photoactivation simulations that are described in the supplemental material. Videos 4 and 5 correspond to Fig. 2, and Videos 6–8 correspond to Fig. 3. Video 9 is a time lapse of p150_CC1 plus a rhodamine-tubulin–injected PtK1 cell (as in Fig. 4 B). Online supplemental material is available at http://www.jcb.org/cgi/content/full/jcb.200601075/DC1.

We thank Sonia Grego and Ben Moree for help setting up the photoactivation laser and the following people for gifts of reagents: Don Cleveland and Tsahai Tafari for antibody to CENP-F; George Patterson and Jennifer Lippincott-Schwartz for PA-GFP plasmid; Duane Compton and Ryoma "Puck" Ohi for antibodies to Kif2a; Jennifer Tirnauer for PtK1 cells expressing GFP-EB1; and Tarun Kapoor for HR22C16-E1 and p150_CC1. We thank Zach Perlman for sharing his image alignment algorithm, Tarun Kapoor and Greg Rogers for insightful comments on the manuscript, and Tim Mitchison and the Marine Biological Laboratory Cell Division Group for stimulating discussions on spindle mechanics.

L.A. Cameron is supported by the American Cancer Society postdoctoral fellowship PF-02-095-01-CCG. This work was supported by the National Institutes of Health grants GM60678 to E.D. Salmon and G. Danuser, GM24364 to E.D. Salmon, and GM59363 to A. Khodjakov.

Submitted: 16 January 2006
Accepted: 16 March 2006

References

Chen, W., and D. Zhang. 2004. Kinetochore fibre dynamics outside the context of the spindle during anaphase. *Nat. Cell Biol.* 6:227–231.

Cimini, D., L.A. Cameron, and E.D. Salmon. 2004. Anaphase spindle mechanics prevent mis-segregation of merotelically oriented chromosomes. *Curr. Biol.* 14:2149–2155.

Danuser, G., and C.M. Waterman-Storer. 2003. Quantitative fluorescent speckle microscopy: where it came from and where it is going. *J. Microsc.* 211:191–207.

DeBonis, S., D.A. Skoufias, L. Lebeau, R. Lopez, G. Robin, R.L. Margolis, R.H. Wade, and F. Kozielski. 2004. In vitro screening for inhibitors of the human mitotic kinesin Eg5 with antimitotic and antitumor activities. *Mol. Cancer Ther.* 3:1079–1090.

Gaetz, J., and T.M. Kapoor. 2004. Dynein/dynactin regulate metaphase spindle length by targeting depolymerizing activities to spindle poles. *J. Cell Biol.* 166:465–471.

Ganem, N.J., K. Upton, and D.A. Compton. 2005. Efficient mitosis in human cells lacking poleward microtubule flux. *Curr. Biol.* 15:1827–1832.

Goshima, G., R. Wollman, N. Stuurman, J.M. Scholey, and R.D. Vale. 2005. Length control of the metaphase spindle. *Curr. Biol.* 15:1979–1988.

Hill, T.L. 1985. Theoretical problems related to the attachment of microtubules to kinetochores. *Proc. Natl. Acad. Sci. USA*. 82:4404–4408.

Hotha, S., J.C. Yarrow, J.G. Yang, S. Garrett, K.V. Renduchintala, T.U. Mayer, and T.M. Kapoor. 2003. HR22C16: a potent small-molecule probe for the dynamics of cell division. *Angew. Chem. Int. Ed. Engl.* 42:2379–2382.

Kapoor, T.M., T.U. Mayer, M.L. Coughlin, and T.J. Mitchison. 2000. Probing spindle assembly mechanisms with monastrol, a small molecule inhibitor of the mitotic kinesin, Eg5. *J. Cell Biol.* 150:975–988.

Khodjakov, A., and C.L. Rieder. 1996. Kinetochores moving away from their associated pole do not exert a significant pushing force on the chromosome. *J. Cell Biol.* 135:315–327.

LaFountain, J.R., Jr., C.S. Cohan, A.J. Siegel, and D.J. LaFountain. 2004. Direct visualization of microtubule flux during metaphase and anaphase in crane-fly spermatocytes. *Mol. Biol. Cell*. 15:5724–5732.

Maddox, P., A. Straight, P. Coughlin, T.J. Mitchison, and E.D. Salmon. 2003. Direct observation of microtubule dynamics at kinetochores in *Xenopus* extract spindles: implications for spindle mechanics. *J. Cell Biol.* 162:377–382.

Margolis, R.L., and L. Wilson. 1981. Microtubule treadmills–possible molecular machinery. *Nature*. 293:705–711.

McDonald, K.L., E.T. O'Toole, D.N. Mastronarde, and J.R. McIntosh. 1992. Kinetochore microtubules in PTK cells. *J. Cell Biol.* 118:369–383.

McEwen, B.F., Y. Ding, and A.B. Heagle. 1998. Relevance of kinetochore size and microtubule-binding capacity for stable chromosome attachment during mitosis in PtK1 cells. *Chromosome Res.* 6:123–132.

Mitchison, T.J. 1989. Polewards microtubule flux in the mitotic spindle: evidence from photoactivation of fluorescence. *J. Cell Biol.* 109:637–652.

Mitchison, T.J., P. Maddox, A. Groen, L. Cameron, Z. Perlman, R. Ohi, A. Desai, E.D. Salmon, and T.M. Kapoor. 2004. Bipolarization and poleward flux correlate during *Xenopus* extract spindle assembly. *Mol. Biol. Cell*. 15:5603–5615.

Miyamoto, D.T., Z.E. Perlman, K.S. Burbank, A.C. Groen, and T.J. Mitchison. 2004. The kinesin Eg5 drives poleward microtubule flux in *Xenopus laevis* egg extract spindles. *J. Cell Biol.* 167:813–818.

Patterson, G.H., and J. Lippincott-Schwartz. 2002. A photoactivatable GFP for selective photolabeling of proteins and cells. *Science*. 297:1873–1877.

Ponti, A., P. Vallotton, W.C. Salmon, C.M. Waterman-Storer, and G. Danuser. 2003. Computational analysis of F-actin turnover in cortical actin meshworks using fluorescent speckle microscopy. *Biophys. J.* 84:3336–3352.

Pratt, W.K. 2001. Digital Image Processing: PIKS Inside. Wiley-Interscience, New York. 735 pp.

Rieder, C.L., and E.D. Salmon. 1998. The vertebrate cell kinetochore and its roles during mitosis. *Trends Cell Biol.* 8:310–318.

Rogers, G.C., S.L. Rogers, T.A. Schwimmer, S.C. Ems-McClung, C.E. Walczak, R.D. Vale, J.M. Scholey, and D.J. Sharp. 2004. Two mitotic kinesins cooperate to drive sister chromatid separation during anaphase. *Nature*. 427:364–370.

Rogers, G.C., S.L. Rogers, and D.J. Sharp. 2005. Spindle microtubules in flux. *J. Cell Sci.* 118:1105–1116.

Salmon, E.D. 2005. Microtubules: a ring for the depolymerization motor. *Curr. Biol.* 15:R299–R302.

Sawin, K.E., and T.J. Mitchison. 1991. Poleward microtubule flux mitotic spindles assembled in vitro. *J. Cell Biol.* 112:941–954.

Shirasu-Hiza, M., Z.E. Perlman, T. Wittmann, E. Karsenti, and T.J. Mitchison. 2004. Eg5 causes elongation of meiotic spindles when flux-associated microtubule depolymerization is blocked. *Curr. Biol.* 14:1941–1945.

Tirnauer, J.S., J.C. Canman, E.D. Salmon, and T.J. Mitchison. 2002. EB1 targets to kinetochores with attached, polymerizing microtubules. *Mol. Biol. Cell*. 13:4308–4316.

Waterman-Storer, C.M., A. Desai, J.C. Bulinski, and E.D. Salmon. 1998. Fluorescent speckle microscopy, a method to visualize the dynamics of protein assemblies in living cells. *Curr. Biol.* 8:1227–1230.

Waters, J.C., T.J. Mitchison, C.L. Rieder, and E.D. Salmon. 1996. The kinetochore microtubule minus-end disassembly associated with poleward flux produces a force that can do work. *Mol. Biol. Cell*. 7:1547–1558.

Zhai, Y., P.J. Kronebusch, and G.G. Borisy. 1995. Kinetochore microtubule dynamics and the metaphase-anaphase transition. *J. Cell Biol.* 131:721–734.

JCB Online Supplemental Material

Cameron et al., http://www.jcb.org/cgi/doi/10.1083/jcb.200601075/DC1

Speckle detection and tracking

Image alignment.

Alignment was performed on cropped images of the spindle without segmenting the speckled region. For a given image sequence $I_1,...I_k,...I_N$, the translation and rotation between consecutive frames were calculated using a standard correlation-maximization algorithm (Pratt, 2001). Specifically, if we denote the aligned image of I_{k-1} by I'_{k-1}, spindle motion between I_k and its aligned preceding frame I'_{k-1} was approximated locally using a linear transformation

$$T_k = \begin{bmatrix} R_k & 0 \\ D_k & 1 \end{bmatrix}$$

that maximizes the correlation between I_k and I'_{k-1}, where R_k and D_k denote spindle rotation and translation, respectively.

Speckle detection.

Speckle detection was performed on the aligned images as previously described (Ponti et al., 2003). When out of focus fluorescence was significant, the coefficient in the shot noise model was set to zero in order to avoid the influence of model inaccuracy.

Speckle tracking.

A new particle-tracking algorithm was developed for fluorescent speckle microscopy (Yang, G., A. Matov, and G. Danuser. 2005. Proceedings of the Institute of Electrical and Electronics Engineers International Conference on Computer Vision and Pattern Recognition. 9–17). In brief, speckle tracking was formulated as a modified bipartite graph linear assignment problem and was solved using the Jonker-Volgenant algorithm (Jonker and Volgenant, 1987)

$$\begin{aligned} &\hat{a}^k = \arg\max_{a^k} \sum_{i\in G_k} \sum_{j\in G_{k+1}} a^k(i,j)\, c^k(i,j)\, p\left(i,j,F(i)\right) \\ &st.\ \ \sum_i a^k(i,j) = 1,\ \sum_j a^k(i,j) = 1,\ \ a^k(i,j) \in \{0,1\} \end{aligned} \qquad (1)$$

where $a^k(i,j)$ denotes the unknown assignment matrix. $a^k(i,j)=1$ if and only if element *i* in subgraph G_k is assigned to element *j* in subgraph G_{k+1}. Subgraph G_k and G_{k+1} consist of all detected speckles in frame *k* and *k* + 1, respectively. $c^k(i,j)$ denotes the association cost of assigning speckle *i* to speckle *j*. This cost is weighed by the probability for linking *i* to *j* given the global speckle flux vector field $F(\cdot)$ at speckle *i*, which is denoted $p(i,j,F(i))$.

Definition of speckle flux vector field.

The vector field of speckle flux is required to solve Eq. 1. For this purpose, a more robust version of the graph algorithm described in Vallotton et al. (2003) was developed (Yang, G., A. Matov, and G. Danuser. 2005. Proceedings of the Institute of Electrical and Electronics Engineers International Conference on Computer Vision and Pattern Recognition. 9–17). This algorithm exploits the speckles in three consecutive frames to establish smooth motion in the flux field. However, because of the small size of PtK1 spindles, the relatively low number of speckles, and the short speckle lifetime, the flux vector field *F* could not be computed reliably. Instead, the flux field was defined interactively based on spindle geometry. An example (a monastrol-treated monopolar spindle) is shown in Fig. S1 A. After the pole center C_0 (shown in red in Fig. S1 B) was defined, the speckle flux vector at position X_k was computed as

$$F(X_k)=\frac{C_0-X_k}{\|C_0-X_k\|}.$$

A deviation tolerance angle, set to be between 45 and 60°, was used to accommodate the inaccuracy of this simplified approximation of spindle geometry and the randomness of speckle motion. For a given track *i* that consists of the point sequence of $X_{i,0},X_{i,1},\ldots,X_{i,N}$, its flux rate V_i is defined as its mean velocity; namely, the ratio between total speckle displacement and time (Fig. S1 C):

$$V_i=\frac{\sum_{j=1}^{N}\left\|X_{i,j}-X_{i,j-1}\right\|_2}{N}.$$

Limits of accuracy in tracking speckles in PtK1 spindle fibers produced by the short lifetime of non-KMTs

Because of the short lifetime of nonkMTs, we had to sample one frame every 10 s or faster to guarantee that speckles associated with nonkMTs have a mean speckle lifetime of approximately three frames, which is necessary for reliable tracking. However, this constraint works against the requirements for time sampling imposed by the limited spatial resolution we could afford. Because of the low photon number produced by the few fluorophores per speckle, we were obligated to apply 2 × 2 pixel binning to capture a fluorescent signal significantly above camera noise. This restricted the effective pixel size to 0.13 μm in object space. Under this condition, 10-s sampling is the fastest rate in which an instantaneous speckle velocity of 0.7 μm/min can be captured (assuming a speckle localization error of ∼0.5 pixels). Together, these calculations indicate that qFSM of MT flux in PtK1 spindles reaches the limits of fluorescence imaging and tracking technology.

Photoactivation simulation

To study whether spatial heterogeneity of MT flux can be revealed by photoactivation measurements, we performed a series of simulation experiments in which flux rates of tubulin marks were assumed to follow normal distributions. The results are summarized as follows (see Video 3). (1) Simulation results confirm that the difference in mean MT flux among different fibers is small. The first part of the video PAsimulation_case1 simulates the case when there is no variation in MT flux between different fibers and within each individual fiber (the mean flux rate is set to be 0.65 μm/min). In comparison, the next section of the video PAsimulation_case2 simulates the case when there is a SD of 0.27 μm/min in flux rates between different fibers but no variation within a fiber. This simulation shows that if the variations in flux rate were mainly caused by different flux rates in different fibers, the activated fluorescent bar across several fibers would have gradually disintegrated into multiple blobs. It is clear from actual photoactivation videos that the fluorescent bar across different fibers remained largely intact. This indicates that the flux rates along different fibers are similar. (2) Simulation results show that spatial heterogeneity in MT flux cannot be observed from photoactivation videos. The third part of the video, PAsimulation_case3, simulates the case when there is no variation in flux between different fibers but flux varies within a fiber with a SD of 0.27 μm/min. No significant differences can be observed between PAsimulation_case1 and PAsimulation_case3. The last section of the video, PAsimulation_case4, simulates the case when there are two modes in MT flux distribution: a total of 75% of the fluorescent marks obey normal velocity distribution of $N(0.65,0.27)$ and remain active throughout the video, whereas the remaining 25% of fluorescent tubulin marks obey a normal velocity distribution of $N(0.33,0.27)$ and disappear after the first five frames. Except for the relatively small elongation of the blobs in the first five frames, no difference can be observed between this video and PAsimulation_case3. It would be very difficult to fully recover the two-mode distribution using only photoactivation data because the responses of those short lifetime events of a small population can be easily masked by the rest.

Comparison of flux distribution in monastrol-treated bipolar spindles with monastrol-treated monopolar spindles

We compared the flux distribution of bipolar spindles with monopolar spindles in cells treated with 100 μM monastrol by computing their cumulative probability distribution (Fig. S1 D). The cumulative distribution is essentially free of influences from the discrete spatial and temporal sampling observed in this specific group of data (effective pixel size is 0.13; frame rate is 10 s/frame; see inset histogram of monastrol-treated bipole). For each spindle configuration, data from two videos are pooled together to increase the number of samples. The number of tracks used to compute monastrol bipole distribution is 138 (Fig. S1 D, red); the number of tracks used to compute monastrol monopole distribution is 242 (Fig. S1 D, green). The distributions show that there are a higher percentage of tracks with low flux rate in monastrol-treated bipole than in monastrol-treated monopole. By performing a Kolmogorov-Smirnov test of the two distributions, we get a P value of 0.0167, indicating that the distributions are different. However, the mean flux values are statistically indistinguishable (0.56 ± 0.25 μm/min for monastrol-treated bipole; 0.57 ± 0.35 μm/min for monastrol-treated monopole). We conjecture that the difference between the two configurations originate in the overlap that is still present in the monastrol-treated bipole. Although its ATPase activity is blocked, kinesin 5 may act as a partial cross-linker between oppositely oriented MT fibers and, thus, oppose the pulling-in mechanism in driving poleward flux. Kinesin 5–mediated cross-linking of oppositely oriented MTs is absent in a monopole (compare with Fig. 3 A). This model needs verification in larger spindles where the degree of overlap can be measured accurately.

References

Jonker, R., and A.Volgenant. 1987. A shortest augmenting path algorithm for dense and sparse linear assignment problems. *Computing*. 38:325–340.

Ponti, A., P. Vallotton, W.C. Salmon, C.M. Waterman-Storer, and G. Danuser. 2003. Computational analysis of F-actin turnover in cortical actin meshworks using fluorescent speckle microscopy. *Biophys. J*. 84:3336–3352.

Pratt, W.K. 2001. Digital Image Processing: PIKS Inside. Wiley-Interscience, New York. 735 pp.

Vallotton, P., A. Ponti, C.M. Waterman-Storer, E.D. Salmon, and G. Danuser. 2003. Recovery, visualization, and analysis of actin and tubulin polymer flow in live cells: a fluorescent speckle microscopy study. *Biophys. J*. 85:1289–1306.